Journal of Catalysis **191,** 116–127 (2000)
doi:10.1006/jcat.1999.2779, available online at http://www.idealibrary.com on IDEAL®

Increased Sulfur Tolerance of Pt/KL Catalysts Prepared by Vapor-Phase Impregnation and Containing a Tm Promoter

Gary Jacobs, Firoz Ghadiali, Adriana Pisanu, Cristina L. Padro,[2] Armando Borgna,[2] Walter E. Alvarez,[3] and Daniel E. Resasco[1]

School of Chemical Engineering, University of Oklahoma, Norman, Oklahoma 73019

Received August 10, 1999; revised December 8, 1999; accepted December 8, 1999

Tm-containing Pt/KL catalysts were prepared by a variety of techniques, including incipient wetness impregnation (IWI), ion exchange (IE), and vapor-phase impregnation (VPI) methods. The Pt morphology resulting from the addition of Tm and Pt sequentially, using the VPI method, was found to yield the greatest enhancement to the aromatization performance of the Pt/KL catalysts studied. The presence of Tm in the sequential VPI Pt/Tm/KL catalyst resulted reproducibly in a catalyst with higher Pt dispersion than that in an unpromoted VPI catalyst, as determined by EXAFS analysis and DRIFTS of adsorbed CO. VPI catalysts give more finely dispersed Pt clusters than either conventional IWI or IE methods. From TPO of poisoned catalysts, Tm was also found to act as a getter for sulfur, so it delays the poisoning of Pt under sulfur-containing feeds, as further evidenced by reaction studies. In addition, the initial activity of the Tm-promoted VPI catalysts was found to be higher than that of the unpromoted Pt/KL VPI catalysts, suggesting that Tm may directly modify Pt or even participate in accelerating the aromatization reaction. The amount and method of incorporation of Tm were found to be critical to the morphology of the Pt clusters and, subsequently, to catalyst performance under sulfur-free and sulfur-poisoned reaction conditions. While the sequential vapor-phase impregnation method with a small amount of Tm (0.15%) yielded a catalyst with improved catalytic properties, some of the other methods such as coimpregnation of Pt and Tm were found to hinder the dispersion of Pt. This may cause the blocking of the L-zeolite channels, as demonstrated by DRIFTS of adsorbed CO, and a higher deactivation rate in the reaction. © 2000 Academic Press

Key Words: **Pt/KL; aromatization; *n*-hexane; EXAFS; DRIFTS; vapor-phase impregnation; lanthanide promoters; chemical vapor deposition.**

INTRODUCTION

Pt/KL catalysts are highly active and selective for the aromatization of hexane (1, 2), but they display a very high sensitivity to even small concentrations of sulfur in the feed (3). It has been shown that in the presence of less than 1 ppm sulfur, the catalysts deactivate in hours (4, 5). This widely recognized sensitivity represents a major obstacle for the utilization of these catalysts in industrial practice (6). Maintaining the required low levels of sulfur to avoid deactivation in commercial operations (i.e., less than about 50 ppb) is certainly expensive. One may expect that the application of these catalysts would be more widespread if they were able to withstand higher sulfur concentrations. Therefore, research in this area may have a remarkable economic impact. Recent studies have focused on understanding the nature of this deactivation. Some authors have suggested that, in the presence of sulfur, Pt particle growth is accelerated, resulting in plugging of the zeolite channels (4, 7). Other authors have proposed that the K cations directly participate in the aromatization process and they, rather than Pt, are preferentially poisoned by sulfur (8).

Few reports have been published on investigations attempting to develop sulfur-tolerant Pt/KL aromatization catalysts (9). One possible approach to increase sulfur tolerance could be the addition of promoters. There are a number of ways in which these promoters could operate (10). They may act as anchoring sites for Pt particles, thus preventing their growth. They may also act as sulfur getters, thus protecting Pt, albeit temporarily, from sulfur poisoning. Alternatively, they might modify the chemical properties of Pt, making it less susceptible to poisoning. For example, the support acidity has in some cases been associated with increased sulfur tolerance (11, 12). The rationale for this tolerance is that, on acidic supports, the metal particles are electron deficient, and this electron deficiency would result in weaker metal–sulfur bonds. In support of this idea, the sulfur coverage has been found to decrease with increasing support acidity (13).

Few authors have studied the addition of rare earth elements as promoters (14–16). Li *et al.* (14, 17) have indicated that the addition of rare earth elements may have a positive effect on the aromatization activity and the sulfur resistance of Pt/KL catalysts. In those studies, the preparation method employed was the coimpregnation of Pt and the rare earth

[1] To whom correspondence should be addressed. E-mail: resasco@ou.edu.

[2] Permanent address: INCAPE, Santiago del Estero 2654 (3000) Santa Fe, Argentina.

[3] Permanent address: INTEMA, Juan B. Justo 4302, (7600) Mar del Plata, Argentina.

0021-9517/00 $35.00

with aqueous solutions. In a recent investigation (18), we have pointed out that by varying the method of preparation of Pt/KL catalysts, one can greatly influence the size and morphology of the Pt particles inside the channels of the zeolite. These morphology variations have strong effects on the stability of the catalysts under both sulfur-free and sulfur-containing feeds. It was observed that, at low Pt loadings, both incipient wetness impregnation (IWI) and vapor-phase impregnation (VPI) methods (19–21) result in the majority of particles being located inside the channels of the L-zeolite. However, the VPI catalysts had smaller particles than those in the catalysts prepared by the IWI method. In addition, EXAFS demonstrated for the VPI series a higher degree of interaction with the L-zeolite framework oxygen atoms. Pulse testing of the methylcyclopentane ring opening showed that the very small clusters produced by the VPI preparation did not result in collimation of the MCP molecule, implying that the reactants and products could easily diffuse over the Pt clusters. This is in contrast to the particles produced by the IWI method, which clearly displayed a collimation effect (22, 18). The characteristic morphology produced by the VPI method was found to improve the performance of the catalyst under clean and sulfur-poisoned conditions, enhancing the catalyst's resistance to the formation of coke and decreasing the particle agglomeration rate. A detailed TEM study has recently been published (23) demonstrating the impact of platinum morphology in Pt/KL on pore blockage by agglomeration and coke production. The best Pt/KL catalysts were found to have the platinum inside the channels in a very well dispersed state. In this contribution, we have investigated the combined effects of the preparation method and the addition of a rare earth (Tm), with a primary focus on the vapor-phase impregnation technique as a means to achieve finely distributed Pt clusters.

EXPERIMENTAL

Catalyst Preparation

The K-LTL-zeolite (series TSZ-500; BET area, 292 m^2/g; SiO_2/Al_2O_3 ratio, 6) was provided by Tosoh Co. Before addition of precursor salts, the K-LTL-zeolite was dried in an oven at 383 K for 12 h and calcined by heating the zeolite for 2 h in a flow of UHP air to 673 K and holding at 673 K in an air flow for 5 h. Platinum was loaded by two methods, incipient wetness impregnation (IWI) and vapor-phase impregnation (VPI). For the thulium-promoted catalyst, Tm and Pt were loaded either sequentially or simultaneously. Table 1 summarizes the various catalysts investigated in this work. The preparation parameters investigated were the Tm loading, the method, and the order of incorporating the components. For all preparation methods, the KL-zeolite was first calcined by heating the zeolite for 2 h in a flow of UHP air to 673 K and holding at 673 K in an air flow for 5 h.

TABLE 1

Characteristics of the Catalysts Investigated

Samples	Preparation method	wt% Tm	wt% Pt
IWI	Incipient wetness impregnation	0	1.0
VPI	Vapor-phase impregnation	0	1.0
Tm-s-VPI	Sequential vapor-phase impregnation	0.15	1.0
Tm-S-VPI	Sequential vapor-phase impregnation	1.50	1.0
Tm-co-VPI	Coimpregnation, vapor phase	0.15	1.0
Tm-s-IWI	Sequential incipient wetness impregnation	0.15	1.0
Tm-rs-IWI	Sequential incipient wetness impregnation (reverse sequence)	0.15	1.0
Tm-co-IWI	Coimpregnation, incipient wetness	0.15	1.0
Tm-IE	Tm added by ion exchange, Pt by IWI	0.15	1.0

In the IWI method, the liquid/solid ratio was determined for the L-zeolite to obtain the same degree of incipient wetness in all catalysts. The precursor salt employed was tetraammineplatinum(II) nitrate (Alfa, Stock #88960). Directly after calcination of the zeolite, the sample was impregnated dropwise in an inert He atmosphere to prevent exposure to ambient conditions and filling of the pores with water prior to impregnation. After impregnation of an amount corresponding to 1 wt% Pt, the sample was covered and allowed to stand for 4 h before being dried overnight at 383 K. Finally, to calcine the catalyst, the sample was heated at a rate of 3 K/min to 623 K in an air flow of 100 $cm^3/min\ g_{cat}$, and kept at 623 K in an air flow for 2 h. This calcination procedure was standard for all subsequent impregnation preparations involving Pt and Tm. This sample is identified as IWI.

In the VPI method (21), the precursor employed was platinum(II) 2,4-pentanedionate ($Pt(AcAc)_2$, Alfa, Stock #10526). After calcination of the KL-zeolite to remove chemisorbed water, the solid was then quickly transferred to an inert He atmosphere to prevent condensation of water vapor in the pores. Once transferred, the $Pt(AcAc)_2$ was physically well mixed with the KL-zeolite. First, the salt was stirred uniformly with the zeolite, and then the mixture was ground together. The solid mixture was loaded into a reactor tube, which was sealed under high vacuum at 333 K and evacuated overnight to approximately 10^{-5} Torr. Then, the material was heated to 373 K and held for 1 h to sublime the precursor, at which temperature the pressure increased substantially. After sublimation, the temperature of the mixture was increased to 423 K and held for 15 min. At this point, the sample was slightly yellow in color, an indication that the $Pt(AcAc)_2$ did not decompose during the procedure. To effect the decomposition of the precursor, the sample was heated to 623 K in a flow of air for 2 h and calcined at 623 K for 2 h. The final color of the sample was light gray. This sample is identified as VPI.

Seven Tm-containing catalysts were prepared by different methods. Four samples were prepared by impregnation with aqueous solutions of thulium nitrate and tetraammineplatinum(II) nitrate. One of them was prepared by coimpregnation (Tm-co-IWI), one was prepared by sequential impregnation (Tm-s-IWI) where Tm was added prior to Pt addition, and one was prepared in the reverse sequence (Tm-rs-IWI). For sequential impregnation, intermediate drying and calcination steps were conducted before the second precursor was impregnated. The amount of Tm varied, as shown in Table 1. A fourth sample (Tm-IE) was prepared by ion exchanging the Tm and impregnating the Pt salt.

Two samples of different Tm loading were prepared by the VPI method. In this case, the Tm was first incorporated by sublimation of thulium 2,4-pentanedionate (Alfa, Stock #13164), following the same protocol as described earlier. In the final step, Pt was added by the VPI method. These samples are identified as Tm-s-VPI (0.15 wt% Tm) and Tm-S-VPI (1.5 wt% Tm). Finally, a seventh sample (Tm-co-VPI) was prepared by coimpregnation by the vapor-phase method, in which the two precursors were sublimed simultaneously.

Reaction Testing

In the pulse mode, the *n*-hexane reaction was studied using a Pyrex reactor and 0.025 g of sample in each run. The catalysts were reduced *in situ* at 773 K. The reaction was carried out at 723 and 773 K using 100-μl pulses containing around 6.57×10^{-7} mol of *n*-hexane. The carrier gas (35 cm^3/min) used was hydrogen. The products were analyzed in a Hewlett-Packard 5890 gas chromatograph, equipped with a FID detector and a packed column, 30% DC200-Chromosorb 60/80P AW from Alltech.

In the flow mode, reaction tests were conducted near atmospheric pressure using a fixed-bed, single-pass, continuous-flow reactor. The reactor consisted of a 0.5-in. stainless steel tube with an internal K-type thermocouple. Experiments were conducted at WHSV $= 10\ h^{-1}$ and employed 0.40 g of catalyst in each run. The catalyst bed was supported on a bed of quartz glass wool. The reactor was operated under flowing hydrogen, and *n*-hexane (Aldrich, 99+% purity, <50 ppb sulfur, measured) was added by infusion with a syringe pump (Sage model M365) through a T-junction prior to the reactor. In all experiments, the hydrogen/*n*-hexane ratio was kept at 6.0. Prior to reaction, the catalyst was slowly ramped in flowing hydrogen at 100 cm^3/min for 2 h to a temperature of 773 K and reduced *in situ* under these conditions. All reactions were conducted at 773 K. For sulfur poisoning studies, thiophene was mixed into the *n*-hexane feed prior to reaction.

A purge valve was used to send samples to a gas chromatograph/mass spectrometer (Hewlett-Packard G1800A GCD system) for analysis. The gas chromatograph utilizes helium as the carrier gas and sends purged products of reaction through the column (HP-PLOT/Al_2O_3 "S" Deactivated) to achieve product separation. Finally, products were ionized by the mass spectrometer, which incorporates an electron ionization detector (EID). A temperature ramp program provided the means for adequate peak separation in the GC column. To determine the signal/abundance ratio and quantify the concentration of each component in the products, normalization curves were obtained using pure compounds.

Catalyst Characterization

EXAFS data on *in situ*-reduced samples were obtained at the National Synchrotron Light Source (NSLS) at Brookhaven National Laboratory, Upton, NY, using beam line X-18b equipped with a Si (111) crystal monochromator. The X-ray ring at the NSLS has an energy of 2.5 GeV and a ring current of 80–220 mA. EXAFS data were taken near the L_{III}-edge of Pt (11,564 eV). The experiments were conducted in a stainless steel sample cell, which allowed *in situ* treatments at temperatures ranging from 773 K to liquid nitrogen temperature. Before each measurement, the catalysts, previously reduced *ex situ* at 773 K, were re-reduced *in situ* at 573 K (heating ramp of 10 K/min) for 30 min in flowing H_2. The EXAFS spectra were recorded at liquid nitrogen temperatures under a H_2 flow. Six scans were recorded for each sample. The average spectrum was obtained by adding the six scans. The pre-edge background was subtracted by using power series curves. Subsequently, the post-edge background was removed using a cubic spline routine. The spectra were normalized by dividing by the height of the absorption edge. To avoid overemphasizing the low-energy region (24), the χ data were k^3-weighted. The range in *k*-space utilized to do the analysis was 3.5–13.5 A^{-1}. Theoretical references for Pt–Pt and Pt–O bonds were obtained by using the FEFF program from the University of Washington (25, 27). The FEFFIT fitting routine was employed to obtain the structural parameters of the Pt clusters for the fresh and poisoned catalysts. The Debye–Waller factors for each bond type (σ), the edge energy difference (ΔE_0), the coordination number (N), and the difference in bond distances (ΔR) with respect to the theoretical reference were used as fitting parameters.

Infrared spectra (DRIFTS) of adsorbed CO were obtained on a Bio-Rad FTS-40 spectrometer, equipped with a MCT detector. The experiments were conducted in a diffuse reflectance cell from Harrick Scientific, type HVC-DR2, with ZnSe windows that allowed us to perform *in situ* reduction pretreatments. For each IR spectrum, taken at a resolution of 8 cm^{-1}, 128 scans were added. Prior to each spectrum, the catalyst was re-reduced in a flow of H_2 at 573 K and purged in He for 30 min. Then, the catalyst was exposed to a flow of 3% CO in He for 30 min at room temperature and purged in He for 30 min.

Temperature-programmed oxidation (TPO) of the spent catalysts was performed in a continuous flow of 5% O_2/He while the temperature was linearly increased. The reaction was conducted in a quartz fixed-bed reactor and 40–50 mg of spent catalyst was supported on a bed of quartz glass wool. The catalyst was flushed in He at least for 30 min before the TPO was performed. The evolution of CO_2 produced by the oxidation of the carbon species was monitored by a mass spectrometer. Quantification of the CO_2 produced was calibrated with 100-μl pulses of pure CO_2. The evolved CO_2 partial pressure was normalized by the total pressure and the maximum signal in the pulses of CO_2.

RESULTS AND DISCUSSION

Catalytic Activity Measurements

(a) n-Hexane aromatization in a pulse reactor. In a pulse reactor, a small amount of *n*-hexane is passed over the catalyst under pure hydrogen carrier. Therefore, particularly at the lower temperatures, the pulse results represent the behavior of a bare catalyst, free of preadsorbed hydrocarbons or coke deposits. In this case, the pulse reactor was used to compare the hexane conversions obtained over fresh samples and on samples that had been exposed for 9 h in the flow reactor to a feed containing 1 ppm sulfur. As described in previous work (5), in addition to the hydrogenolysis (C_1–C_5) products, the main by-products observed during our flow reaction experiments were hexenes. Those experiments were conducted at 773 K and using a H_2 : hydrocarbon ratio of 6 : 1. By contrast, in the pulse experiments conducted in excess hydrogen, which was used as a carrier, the main by-products were MCP, 2MP, and 3MP. Table 2 summarizes the overall conversions and selectivities towards aromatization, isomerization, and hydrogenolysis products at 673 and 773 K.

TABLE 2

***n*-Hexane Conversion in the Pulse Reactor**

Catalyst	T (K)	X (%)	S_{Aro}[a]	S_{Iso}[b]	S_{Hydr}[c]
		Fresh Catalysts			
IWI	673	38	32	54	14
VPI	673	46	33	52	15
Tm-s-VPI	673	32	35	50	15
IWI	773	100	70	0	30
VPI	773	100	73	0	26
Tm-s-VPI	773	100	79	0	20
		2 ppm S-Poisoned Catalysts			
IWI	773	10	44	43	13
VPI	773	90	69	8	23
Tm-s-VPI	773	90	68	14	18

Note. Carrier gas, H_2; flow rate, 35 cm^3/min; catalyst amount, 0.025 g.
[a] Selectivity to aromatization (mol%).
[b] Selectivity to isomerization (mol%).
[c] Selectivity to hydrogenolysis (mol%).

In agreement with our previous work (18), we see here that at 673 K, the fresh catalysts did not show great differences in activity or selectivity in the pulse reactor. At the moderate conversions obtained at this temperature, the selectivity toward isomerization products was significant. However, at 773 K, the conversion for the three catalysts was 100%. At this high conversion, the isomerization products are further converted to either benzene or hydrogenolysis products. The interconversion of the C6 products has been previously observed by other authors (28), who incorporated the concept of *ultimate selectivity* to differentiate between the conversion to compounds that at high enough conversions may lead to benzene, and the irreversible hydrogenolysis to C_1–C_5 products. Under these conditions, a moderate improvement in benzene selectivity at 773 K is observed on the VPI and Tm-s-VPI catalysts compared to that on IWI. This difference is even more pronounced on the poisoned catalysts. As can be seen in the Table 2, at 773 K the conversion was only 10% on the IWI catalyst, while it stayed very high for the other two.

(b) n-Hexane aromatization in a flow reactor. The aromatization of *n*-hexane was conducted in the flow reactor at 773 K, keeping a H_2/*n*-hexane feed ratio of 6 and a space velocity of 10 h^{-1} over the three catalysts IWI, VPI, and Tm-s-VPI. During the first 9 h on stream, the feed contained no sulfur. After that initial period, 2 ppm sulfur was incorporated in the feed. As previously reported (18), the catalyst prepared by the VPI method was more active and selective than that prepared by IWI. An interesting increase in activity with the presence of Tm was also observed. An activity enhancement was also reported by Li *et al.* (17). As the time on stream increased, the advantages of the VPI and Tm-s-VPI catalysts over the IWI catalyst became even more pronounced. Similarly, the VPI and particularly the Tm-s-VPI exhibited significantly higher tolerance to sulfur poisoning. Remarkably, the greatest differences were in benzene selectivity more than in overall conversion. This difference is illustrated in Figs. 1a and 1b, which show the variation of the conversion and benzene selectivity with time on stream first under sulfur-free conditions, and subsequently in the presence of 2 ppm S, for each of the three catalysts.

As mentioned above, the main products obtained under the conditions of our flow reaction studies were benzene, hexenes, and hydrogenolysis products ($<C_5$). Isomerization products, which were more abundant in the pulse reactor, were in this case present in only minor concentrations. The hydrogenolysis products were always low for all the catalysts. For example, the highest methane yield barely exceeded 1%. As previously observed, the evolution of methane yield followed a deactivation pattern parallel to that of aromatization (5). In contrast, the production of

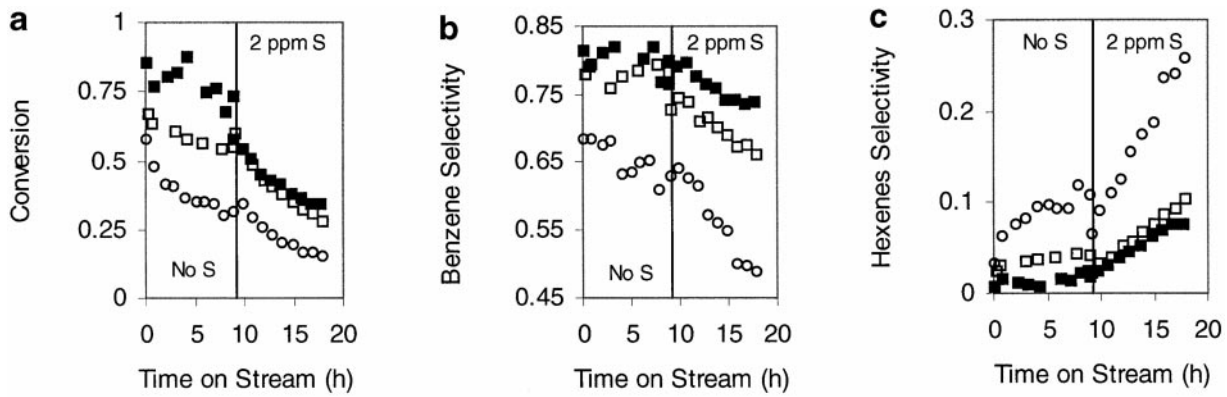

FIG. 1. Variation of the (a) conversion, (b) benzene selectivity, and (c) hexenes selectivity with time on stream first in sulfur-free conditions, and then in the presence of 2 ppm S, for the IWI (open circles), the VPI (open squares), and Tm-s-VPI (filled squares), respectively, at 773 K (WHSV, 10 h^{-1}).

hexenes by dehydrogenation increased with time on stream and this increase was more pronounced when the catalyst deactivated by sulfur poisoning. This behavior is illustrated in Fig. 1c. In good agreement with previous studies (5), it was observed that the catalysts that exhibited the highest aromatization activity produced the lowest amount of hexenes. The VPI sample and particularly the Tm-s-VPI sample produced very little hexenes. Only after deactivation by sulfur suppressed the aromatization activity, the hexene yield became significant.

In the presence of 2 ppm S, the thulium-promoted VPI catalyst showed superior aromatization activity in comparison with the unpromoted VPI and IWI catalysts. However, 10 ppm S was enough to cause all three catalysts to completely lose their ability for aromatization. While the IWI catalyst deactivated completely in 6 h, the Tm-s-VPI and VPI deactivated completely in 8 h. The activity and selectivity for aromatization during poisoning followed the trend Tm-s-VPI > VPI > IWI. It is also interesting to note that the Tm-s-VPI catalyst still retained a high degree of dehydrogenation activity after the aromatization activity was completely lost.

When the Tm-promoted catalysts prepared by different methods were compared, the ones prepared by sequential VPI exhibited the best performance. Both the Tm-s-VPI and Tm-S-VPI catalysts were much more active, selective, and sulfur tolerant than the others. Figure 2 illustrates the behavior of the Tm-s-VPI compared to those of the Tm-co-VPI and Tm-s-IWI, showing that the addition of Tm alone does not guarantee a good performance. Similarly, Fig. 3 (top) makes a comparison of the selectivity vs conversion patterns for the preferred Tm-s-VPI preparation with the ones prepared by the other methods. Plotting selectivity versus conversion is a basis generally accepted as a way to compare Pt/KL catalysts. Figure 3 (bottom) compares our selectivity versus conversion results with some of those found in the literature (21, 41). Both the VPI and Tm-s-VPI catalysts display very high selectivity as a function of conversion, and are among the best reported in the literature.

Table 3 provides a comparison of our results from reaction testing with some results found in the literature. Most authors used different reaction conditions, loadings, and methods of preparation. In comparing our TOF data with those of Fang *et al.* (15), we chose two points of comparison, 4 and 10 h on stream. The catalysts prepared by IWI are relatively in agreement. However, our Tm-s-VPI catalyst presents a significant improvement in comparison to the coimpregnation method used by Fang *et al.* (15).

EXAFS Analysis

A detailed EXAFS analysis of several reduced catalysts was conducted under H_2 flow, before and after 30-h reactions under 1 ppm sulfur (WHSV, 10 h^{-1}). The structural parameters were determined by a fitting procedure, applying an inverse Fourier transform over the *r* range 1.5–3.6 Å

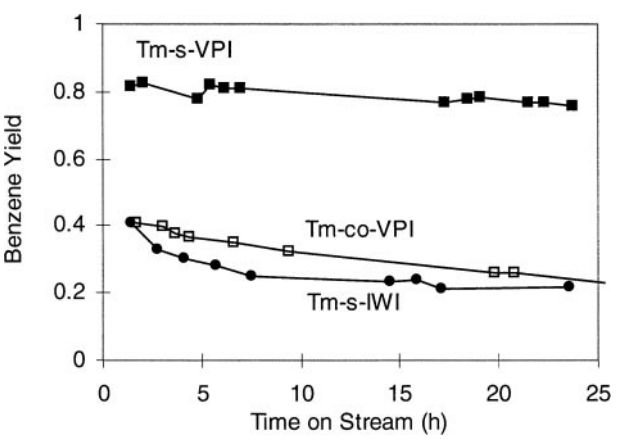

FIG. 2. Yield of benzene as a function of time on stream (WHSV, 5 h^{-1}) for Tm-s-VPI, Tm-co-VPI, and Tm-s-IWI catalysts.

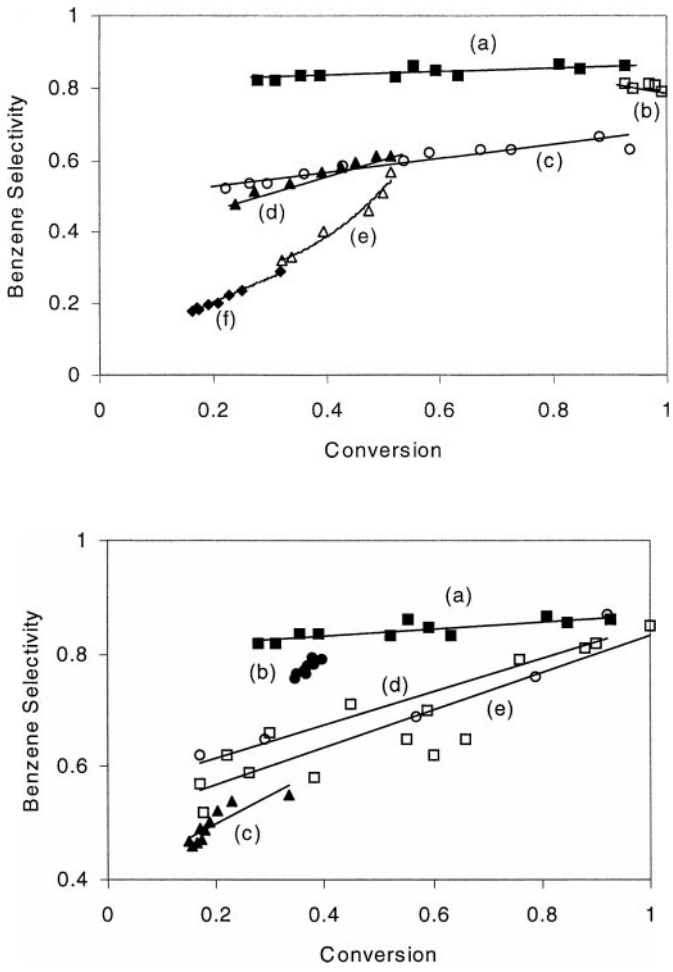

FIG. 3. (Top) Comparison of the selectivity vs conversion patterns for the preferred (a) Tm-s-VPI preparation with the ones prepared by (b) Tm-S-VPI, (c) Tm-s-IWI, (d) Tm-rs-IWI, (e) Tm-IE, and (f) Tm-co-IWI. (Bottom) Comparison of the selectivity vs conversion patterns for our (a) Tm-s-VPI, (b) VPI, and (c) IWI catalysts with those found in the literature including (d) Jentoft *et al.* (41) and (e) Mielczarski *et al.* (21).

to isolate the EXAFS contribution of the first coordination sphere of platinum. According to the Nyquist theorem (29) and the EXAFS specific modifications described by Stern (30), the maximum number of parameters that can be used to describe the EXAFS function is given by the following equation:

$$n_{\max} = 2\Delta k \Delta r/\pi + 2.$$

Therefore, the use of up to nine parameters to fit the data is statistically justified, since for the k and r ranges employed in this work, the Nyquist criterion would allow up to 15 parameters. The filtered data were fitted using the FEFFIT program (31). The data were fitted using theoretical standards generated by the FEFF package (25–27). The quality of the fit was determined by using the *R*-factor, which gives a sum-of-squares measure of the fractional misfit. Therefore, the smaller the *R*-factor, the better the fit is. For good fits, the *R*-factor is always less than or about 2%. Although the fits obtained with only one Pt–Pt coordination could be considered satisfactory for the IWI catalyst, poor fits were obtained for the other samples with higher metal dispersion, as indicated by the *R*-factor values in Table 4. Therefore, more complex models were also studied. New fittings were conducted including an interaction between the Pt and the L-zeolite oxygen atoms (Pt–O bond) for Pt particles inside the channels of the L-zeolite (7, 32). Theoretical amplitudes and phase shifts corresponding to the Pt–O distances were derived with FEFF, assuming Pt–O bonds at 2.56 Å. It has been suggested that these Pt–O interactions are affected by the presence of H_2 in the interfacial layer between the Pt particles and the zeolite walls (33). A second model was also investigated. Because the structure of the smallest Pt particles may be more complex, we incorporated a second type of Pt–Pt bond, corresponding to shorter Pt–Pt bonds existing in the smallest particles. It is conceivable that the samples with very high

TABLE 3

Comparison of Flow-Mode Reaction Testing

Reference	% Pt	% Tm	T (K)	P (atm)	Method	H_2/HC	% Bz yield	% Bz selec.	TOS (h)	TOF(s^{-1})[a] at T (K)
(42)	0.6	0	733	1	IE	6	40	80	1	0.36
(4)	0.6	0	783	8.1	IE Pell	6	67	75	20	0.46
(17)	0.8	0	773	1	IWI	4	35	—	4	0.09
(17)	0.8	0	773	1	IWI	4	30	—	10	0.08
(17)	0.8	0.20	773	1	Co-IWI	4	80	—	4	0.20
(17)	0.8	0.20	773	1	Co-IWI	4	80	—	10	0.20
This work	1.0	0	773	1	IWI	6	24	65	4	0.15
This work	1.0	0	773	1	IWI	6	18	61	10	0.12
This work	1.0	0	773	1	VPI	6	55	78	4	0.34
This work	1.0	0	773	1	VPI	6	45	75	10	0.28
This work	1.0	0.15	773	1	Tm-s-VPI	6	62	82	4	0.39
This work	1.0	0.15	773	1	Tm-s-VPI	6	60	80	10	0.38

[a] Turnover frequency in molecules of benzene turned over per Pt atom per second.

TABLE 4

Changes in Fit Quality with Addition of Contributions

Fitting	E_0	σ^2	N_{Pt-Pt}	N_{Pt-O}	R (Å)	R-factor (%)
			VPI			
1 Pt–Pt distance	1.8	0.0080	6.7	—	2.71	3.4
1 Pt–Pt distance +	0.05	0.0054	3.7	—	2.69	
Pt–O distance		0.0015	—	1.7	3.0	3.3
2 Pt–Pt distances	6.1	0.0028	2.4	—	2.80	1.7
		0.0028	3.1	—	2.68	
2 Pt–Pt distances +	8.6	0.0025	2.1	—	2.81	1.4
Pt–O distance		0.0025	2.7	—	2.69	
		0.0020	—	0.6	2.67	
			Tm-s-VPI			
1 Pt–Pt distance	0.04	0.0097	6.35	—	2.69	17.0
1 Pt–Pt distance +	12.5	0.0077	2.6	—	2.74	13.0
Pt–O distance		0.00001	—	1.5	2.68	
2 Pt–Pt distances	2.3	0.0011	2.0	—	2.77	7.2
			2.1	—	2.65	
2 Pt–Pt distances +	−5.1	0.0012	2.2		2.74	2.8
Pt–O distance		0.0012	2.1		2.61	
		0.0021		1.1	2.39	

TABLE 5

Structural Parameters Determined from EXAFS Analysis

Fitting	E_0	σ^2	N_{Pt-Pt}	N_{Pt-O}	R (Å)	R-factor (%)
IWI, fresh	6.7	0.0056	7.6	—	2.74	1.2
		0.0060	—	0.25	2.73	
IWI, 1 ppm	9.1	0.0056	8.2	—	2.75	0.8
sulfur (30 h)		0.0030	—	0.35	2.71	
VPI, fresh	8.6	0.0025	2.1	—	2.81	1.4
		0.0025	2.7	—	2.69	
		0.0020	—	0.6	2.67	
VPI, 1ppm	5.4	0.0020	3.1	—	2.77	2.6
sulfur (30 h)		0.0020	2.6	—	2.67	
		0.0045	—	0.5	2.67	
Tm-s-VPI, fresh	−5.1	0.0012	2.2		2.74	2.8
		0.0012	2.1		2.61	
		0.0021		1.1	2.39	
Tm-s-VPI, 1 ppm	9.1	0.0035	1.9	—	2.80	0.34
sulfur (30 h)		0.0035	2.8	—	2.69	
		0.0036	—	0.95	2.67	

dispersions may contain a fraction of very small Pt particles, with Pt–Pt distances slightly different from those of larger particles. Such a distance contraction has already been reported for highly dispersed systems (18). A third model was investigated combining both the Pt–O contributions and the second Pt–Pt distance.

As shown in Table 4, this last model gave the highest fitting quality, and in some cases, such as Tm-s-VPI, it was the only model which gave an acceptable fit. The structural parameters resulting from the fits of the fresh and poisoned catalysts using the third model (two Pt–Pt distances and one Pt–O distance) are summarized in Table 5. The Fourier transforms of the EXAFS data for the freshly reduced Tm-s-VPI, VPI, and IWI catalysts, together with the 30-h sulfur-poisoned catalysts, are shown in Figs. 4a, 4b, and 4c, respectively. Note the change in scale for each spectrum.

In agreement with our previous study (18), the resulting parameters indicate that the VPI method leads to a metal dispersion higher than that with the IWI and, consequently, to a higher population of Pt clusters in close proximity to the zeolite walls. This trend is manifested by lower Pt–Pt and higher Pt–O coordination numbers in the VPI samples compared to those in the IWI samples. The Tm-s-VPI catalyst exhibited even lower Pt–Pt and higher Pt–O coordination numbers, suggesting that the addition of Tm results in a better dispersion of Pt, in agreement with an earlier study (17). Also, the coordination distances are somewhat lower for this catalyst than for the other Pt/KL catalysts. It is clear that the preparation of the catalyst is critical to

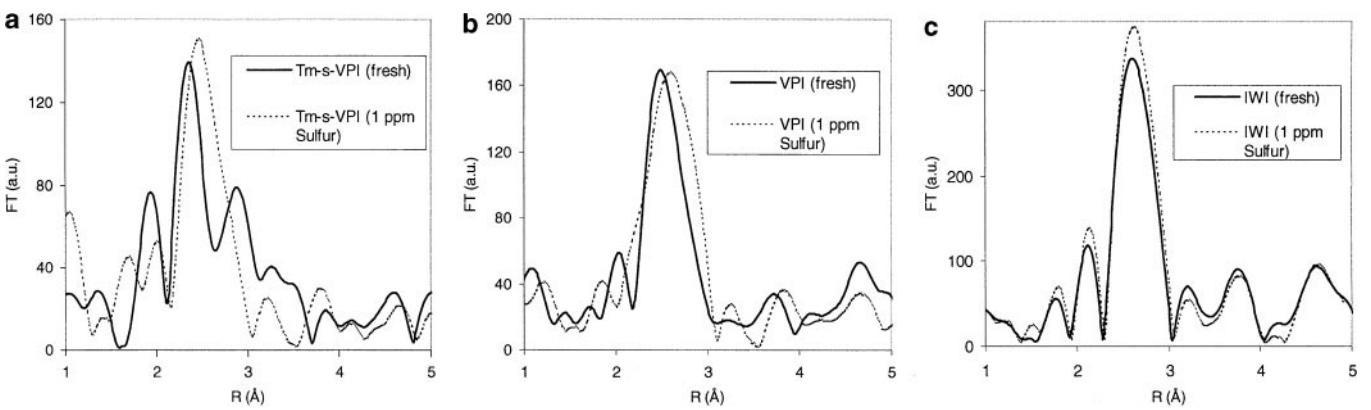

FIG. 4. Fourier transforms of k^3-weighted EXAFS spectra obtained at liquid N_2 temprature on *in situ*-reduced fresh and 30-h, 1 ppm sulfur-poisoned (a) Tm-s-VPI, (b) VPI, and (c) IWI catalysts.

the resulting size and distribution of Pt clusters. This can result in variations between different batches, as noted by comparison with our previous work (18), in which from comparable preparations we obtained a higher metal dispersion. In our experience, the IWI is more sensitive to the preparation than the VPI method (34). Finally, it is important to point out that, regardless of the model used in the EXAFS analysis, the presence of Tm in the Tm-s-VPI catalyst was found to increase the dispersion of the Pt.

By comparing the 30-h, 1 ppm sulfur-poisoned runs, growth is apparent for all of the catalysts. However, the resulting particle size after poisoning by the vapor-phase impregnated catalysts is much smaller than that for the poisoned IWI catalyst. The smallest particle size was retained by the Tm-s-VPI catalyst after poisoning. Previous modeling and TEM studies (4, 23) have shown that after particle growth reaches a point at which two or more channel blockages by Pt occur, a large portion of Pt clusters become entrapped and the catalyst deactivates. Since the IWI catalyst has a fraction of large particles inside the channels of the zeolite, slight growth is enough to cause substantial pore blockage under 30–h, 1 ppm sulfur poisoning. The VPI catalysts, however, and especially Tm-s-VPI still retain high enough dispersion that channel blockage, and, therefore, deactivation, is marginal, as evidenced under reaction testing.

One of the possible explanations given in the literature for the increased activity and sulfur tolerance exhibited by the Tm-promoted catalysts is an electronic modification of Pt due to an electron transfer from Tm. To test this hypothesis, we have analyzed the shape and position of the near-edge structure in the X-ray absorption spectra of the VPI and Tm-S-VPI catalysts, reduced *in situ* and cooled in a hydrogen flow. Figure 5 shows that the shape and position of the two edges are identical, indicating that the presence of Tm does not result in any significant electronic perturbation of Pt.

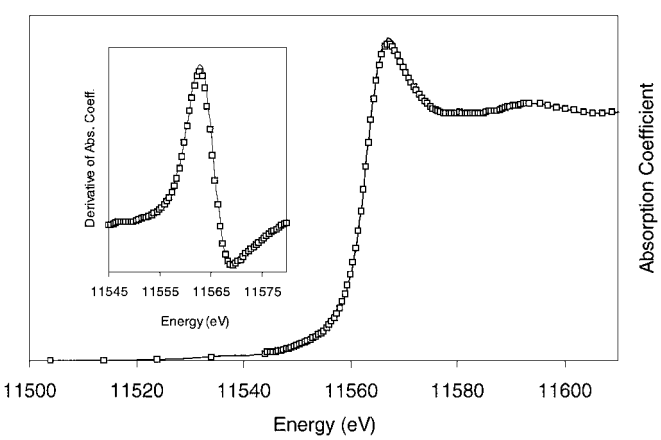

FIG. 5. XANES spectra and derivative of absorption coefficient of Pt L_{III}-edge for VPI (solid line) and Tm-s-VPI (open squares) catalysts.

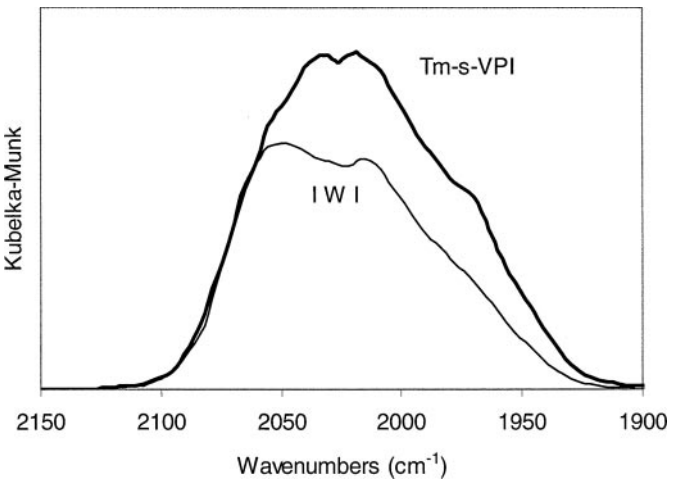

FIG. 6. DRIFTS spectra of CO adsorbed on IWI and Tm-s-VPI catalysts. The reduced catalysts were exposed to a flow of 3% CO in He for 30 min at room temperature and purged in He for 30 min.

DRIFTS of Adsorbed CO

Figure 6 shows the DRIFTS spectra of CO adsorbed on the IWI and Tm-s-VPI catalysts. Important differences are observed. First, in line with a higher metal dispersion, the absorption bands are more intense on Tm-s-VPI than on IWI. Second, the greatest difference in intensity is observed preferentially for the low-frequency bands, i.e., below 2050 cm^{-1}.

Lane *et al.* (35) considered several hypotheses regarding the species responsible for the low-frequency bands. They reported three bands resulting from adsorption of CO: the typical linear band at 2060 cm^{-1}, the bridged band at 1790 cm^{-1}, and an additional low-wavenumber band at 1960 cm^{-1}. They speculated that the support structure influences the location of the platinum and adsorbed CO relative to the potassium cations. From these three bands, they postulated from the position of the potassium and platinum in Pt/KL catalysts that two environments existed for linear bound CO: one oriented through the pore window and a second oriented to a potassium cation near the wall. In support of this idea, the additional band was also apparent on a platinum-supported potassium cation-promoted silica catalyst.

In a previous paper (18), we have employed DRIFTS of adsorbed CO to compare the morphology of Pt particles inside the KL-zeolite, prepared by IWI and VPI methods. In that case, our results agreed very well with a somewhat different hypothesis, that CO itself modifies the structure of the small Pt clusters inside the KL-zeolite (36). For a typical Pt/KL sample, we have observed that during the first few minutes, a band developed centered at about 2068 cm^{-1}. However, only after 10 min did we see new bands emerging at about 2057 and 2014 cm^{-1}. Even later, we saw the formation of additional bands at 1975 cm^{-1} and lower. It was

concluded that CO adsorption does not probe the small metal particles in their original structure, but rather generates by disruption over time new molecular arrangements that are stabilized inside the zeolite.

In support of this idea, Stakheev *et al.* (36) tabulated the reproducibility of the position of these bands from several authors, and suggested that several different molecular species were formed with distinct stoichiometric ratios of Pt_x and CO_y. They proposed that during CO adsorption, Pt carbonyls can be formed and stabilized by the zeolite, which could act as a ligand. EXAFS data (37) have shown that the 5–6-atom metallic particles present in the KL-zeolite before the admission of CO were completely disrupted, and Pt–CO species were formed. Stakheev *et al.* (36) have pointed out that the formation of Pt carbonyls can occur only when the Pt clusters are very small. They indicated that the metal–metal bond strength is much lower than that of the bulk metal only for particles with fewer than 15–20 atoms. Then, one may not expect the Pt particles outside the zeolite to be converted to Pt carbonyls. Therefore, even though CO adsorption alters the structure of the small Pt clusters, FTIR is still a useful technique for making general conclusions about the location (i.e., inside the L-zeolite or external) and the distribution of the Pt clusters prior to disruption.

Although these hypotheses differ regarding the nature of the structures responsible for the low-wavenumber bands (2050–1930 cm^{-1}), all are in general agreement in that they reflect the small Pt clusters inside the channels of the L-zeolite. In contrast, the bands at and above 2075 cm^{-1} are associated with the Pt external to the pores. Bands present between 2050 and 2075 cm^{-1} are likely caused by the Pt clusters in the near-surface region of the L-channels. Supported with other techniques like EXAFS and in correlation with catalytic performance and stability, this technique can be used to characterize the distribution of Pt clusters and their location.

Based on this hypothesis, we can explain the observed differences in the DRIFTS spectra in terms of a higher dispersion of the Tm-s-VPI catalyst, which favors the formation of Pt carbonyls during CO adsorption. The XANES experiments suggest that no significant differences in the electronic state of Pt occur by the addition of Tm. Therefore, the appearance of low-frequency bands should not be ascribed to electronic effects, but rather to a direct interaction of the Pt carbonyls with the cations in the zeolite. The increase in the intensity of the bands in this region is simply a reflection of a greater extent of carbonyl formation/stabilization on the Tm-promoted catalysts, which would have a higher population of ultrasmall particles inside the zeolite than the IWI catalyst. In our previous paper (18), we observed that catalysts treated under a reduction/oxidation/reduction cycle exhibited formation of Pt carbonyls to a much lower extent than freshly reduced catalyst as a result of a particle growth.

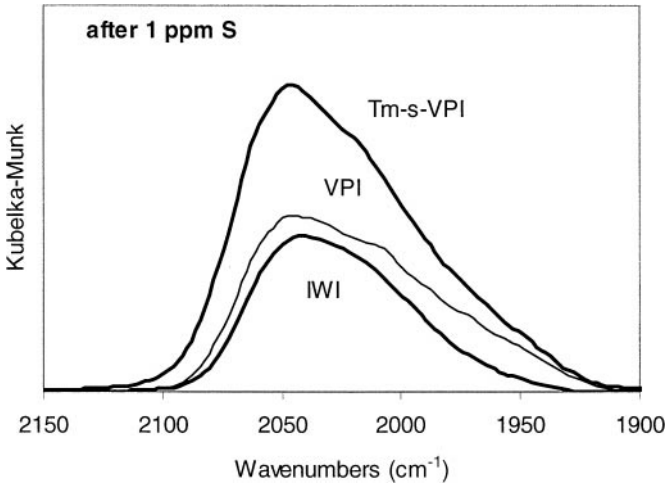

FIG. 7. DRIFTS spectra of CO adsorbed on IWI, VPI, and Tm-s-VPI catalysts after the catalysts were exposed to 9 h of reaction at 773 K, under 1 ppm sulfur (WHSV, 10 h^{-1}). The reduced catalysts were exposed to a flow of 3% CO in He for 30 min at room temperature and purged in He for 30 min.

DRIFTS has also been used to characterize the catalysts after exposure to reaction in the presence of sulfur. Figure 7 compares the spectra of adsorbed CO on the three catalysts IWI, VPI, and Tm-s-VPI after being exposed to 9 h reaction at 773 K, under 1 ppm S. A clear difference is observed for the Tm-promoted catalyst in comparison with the unpromoted ones. The integrated area for the Tm-s-VPI catalyst exposed to 1 ppm S is almost the same as that for the fresh catalyst, indicating that the poisoning of Pt has been minimal. By contrast, a significant reduction in absorbance was observed for the VPI, and even more for the IWI catalyst. The most important effect of sulfur on the Tm-s-VPI catalyst is a decrease in the 1970 cm^{-1} band. As discussed before, this band can be ascribed to carbonyls stabilized by the zeolite cations. Since this band is most intense on the Tm-s-VPI catalyst, it is possible that some of the cations that stabilize the carbonyls responsible for this band may be Tm. The disappearance of this band could indicate that Tm gets poisoned by sulfur, losing the ability to stabilize the carbonyls, but keeping the Pt surface free. When the addition of sulfur exceeds the trapping capacity of Tm, Pt starts being poisoned. This is illustrated in Fig. 8, which shows the spectra of the three samples after exposure to reaction under 10 ppm S. In this case, there is no difference in the DRIFT spectra for the three catalysts.

As noted earlier, the addition of Tm alone does not guarantee an enhancement in catalyst performance. When the Tm-promoted catalysts prepared by different methods were compared, the ones prepared by sequential VPI exhibited the best performance. Figure 9 shows the spectra of adsorbed CO on two Tm catalysts, the Tm-s-VPI

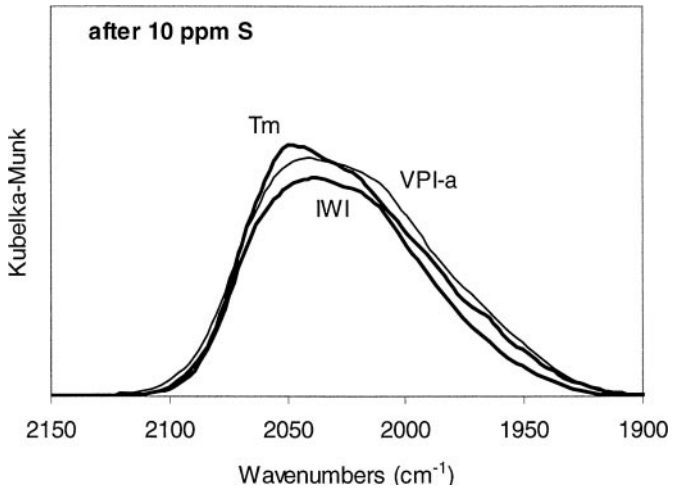

FIG. 8. DRIFTS spectra of CO adsorbed on IWI, VPI, and Tm-s-VPI catalysts after the catalysts were exposed to 9 h of reaction at 773 K, under 10 ppm sulfur (WHSV, 10 h^{-1}). The reduced catalysts were exposed to a flow of 3% CO in He for 30 min at room temperature and purged in He for 30 min.

and the Tm-co-VPI. A clear difference is observed. The Tm-co-VPI catalyst, which exhibited much poorer activity and selectivity than the Tm-s-VPI catalyst, displays a more pronounced shoulder in the region around 2080 cm^{-1}, indicative of linear CO on larger Pt particles. This suggests that the sublimation of both metals simultaneously in the vapor phase leads to blocking of the channels, resulting in a poor dispersion. On the other hand, the Tm-s-VPI catalyst, as described earlier, has a greater fraction of bands at lower wavenumbers where Pt carbonyls form, indicative of very small, well-dispersed Pt.

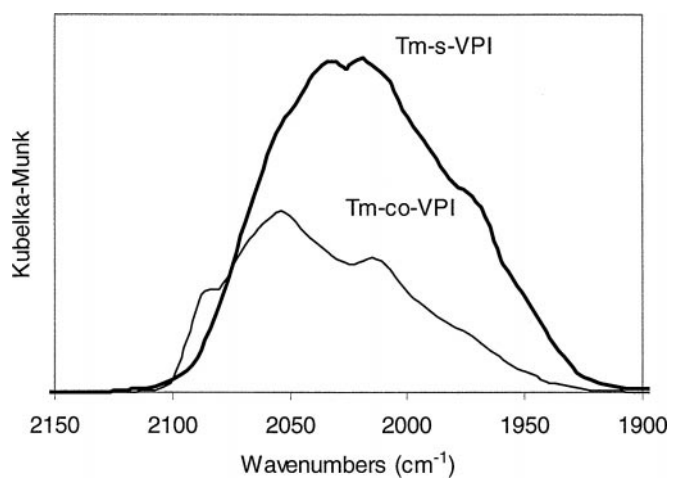

FIG. 9. DRIFTS spectra of CO adsorbed on Tm-s-VPI and Tm-co-VPI fresh catalysts. The reduced catalysts were exposed to a flow of 3% CO in He for 30 min at room temperature and purged in He for 30 min.

TABLE 6

Amount of Carbon Deposited in the *n*-Hexane Aromatization Reaction, as Determined by TPO

Catalyst	% C after 9-h run, S-free	% C after 9-h run, 1 ppm S
IWI	2.7	2.7
VPI	1.1	1.1
Tm-VPI	1.2	1.1

Temperature-Programmed Oxidation (TPO) of Coke Deposits

To characterize the amount and nature of the coke deposited on the different catalysts during runs with and without sulfur, we have conducted TPO measurements on spent samples. Table 6 summarizes the amount of C deposited on each catalyst after 9 h on stream with a sulfur-free feed and with 1 ppm S. Two trends are immediately apparent: (a) the IWI catalysts formed considerably more coke than the two VPI catalysts, and (b) the presence of sulfur in the feed did not have a pronounced effect on the amount of carbon deposited.

That the IWI catalysts form more coke is not surprising. In our earlier work (18), the Pt clusters formed by the IWI procedure were less well-dispersed than those produced by the VPI catalyst. TEM has shown that, though in a very small fraction, some larger Pt clusters outside the channels of the L-zeolite were detected for catalysts prepared by IWI. Iglesia and Baumgartner (38, 39) have shown that in the *n*-hexane aromatization reaction, the Pt that is well-dispersed inside the channels of the L-zeolite is protected from bimolecular collisions which lead to coke formation, while those outside quickly become coked. Furthermore, microcalorimetric studies performed by Sharma *et al.* (40) clearly demonstrated the uniqueness of Pt/KL to resist deactivation by coke. After *n*-hexane aromatization, coking on Pt/silica, which has no protection from microporous channels, was found to suppress adsorption sites much more than a Pt/K(Ba)L catalyst. On the other hand, the amount of coke formed is not affected by the presence of sulfur in the feed because the deactivation of the catalyst by coke deposition occurs during the first several hours on stream, as noted in previous studies (5, 41). The poisoning by sulfur takes a much longer period of time to be observed.

The analysis of the TPO profiles also provides some interesting information that will allow us to further understand the role of Tm. When the profiles of the IWI catalyst used sulfur-free and under 1 ppm S are compared, a clear difference emerges. As shown in Fig. 10, the TPO of the catalyst that was not exposed to S exhibits a prominent carbon oxidation peak at the lower temperature region, which is drastically reduced on the TPO of the sulfur-poisoned sample. We ascribe this low-temperature peak to Pt-catalyzed

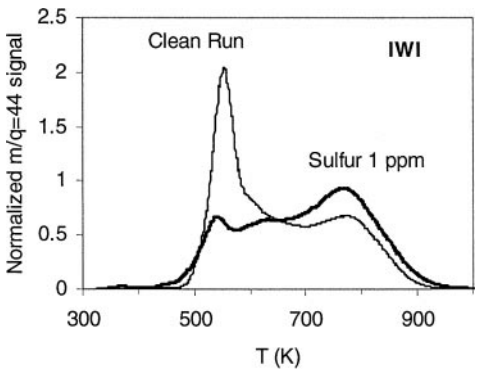

FIG. 10. TPO profiles for the IWI catalyst after a sulfur-free run and a run with 1 ppm sulfur present in the feed.

oxidation. However, on the poisoned catalyst, the oxidation shifted to higher temperatures, while the overall area under the profile remained exactly the same. Similar changes were observed on the Tm VPI and VPI catalysts.

In all cases, the samples that were not exposed to sulfur presented the low-temperature peak, but this peak was greatly reduced on the sulfur-poisoned samples. Since the amount of carbon was almost unchanged, it seems that the presence of sulfur on the poisoned platinum clusters inhibited Pt-catalyzed oxidation of carbon during the TPO, thus shifting it to higher temperatures, rather than modifying the nature of the coke deposits. Based on this premise, the presence of the sharp, low-temperature TPO peak could be taken as a fingerprint for sulfur-free Pt.

To investigate whether Tm may act as a sulfur getter, we prepared reactors which contained three consecutive beds. In the first case, the front and back beds each contained 0.2 g of the VPI catalyst. They were separated by a middle bed, containing 0.4 g of 1.5% Tm/KL. The results obtained in this arrangement were compared to those obtained in a similar reactor in which the middle bed only contained 0.4 g of bare SiO_2. This comparison is illustrated in the TPO profiles of the coke deposits shown in Figs. 11 and 12, obtained after 9 h on stream with a feed containing 2 ppm S. A clear difference is immediately obvious. For the set which had the Tm/KL bed in the middle, the TPO of the bottom bed shows a prominent peak at low temperatures, indicating that the Pt has not been poisoned. However, for the set which had the bare SiO_2 bed in the middle, the TPOs of both bottom and top samples were almost the same, clearly showing that both were almost equally poisoned. These experiments demonstrate that one of the effects of Tm is to capture sulfur, therefore guarding the Pt particles from poisoning.

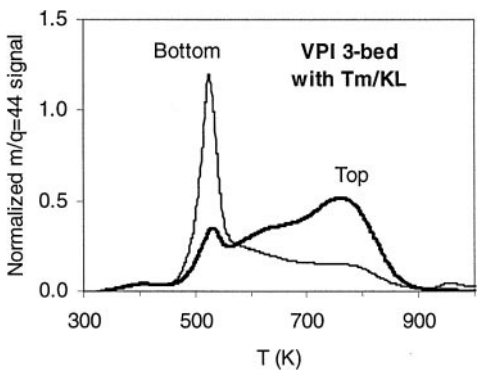

FIG. 11. Three consecutive beds in series, two VPI beds separated by a bed of Tm (1.5%)/KL in the middle. TPO profiles for the top and bottom VPI beds are shown after 9 h on stream (T, 773 K; WHSV, 10 h^{-1}) with a feed containing 2 ppm S.

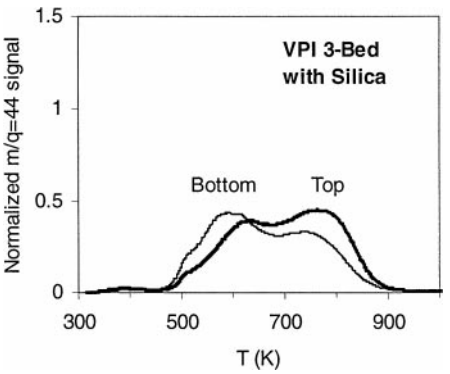

FIG. 12. Three consecutive beds in series, two VPI beds separated by a bed of silica in the middle. TPO profiles for the top and bottom VPI beds are shown after 9 h on stream (T, 773 K; WHSV, 10 h^{-1}) with a feed containing 2 ppm S.

CONCLUSIONS

When prepared correctly, the addition of Tm has important consequences on the aromatization performance of Pt/KL catalysts. There are several ways in which Tm affects the activity, selectivity, and stability of Pt/KL:

(a) The presence of Tm results in a catalyst with higher Pt dispersion. As demonstrated before, a higher dispersion by itself results in a much better catalyst, even without the addition of any promoter.

(b) Tm acts as a sulfur getter, so it delays the poisoning of Pt.

(c) The initial activity of the Tm-promoted catalysts is higher than that of unpromoted Pt/KL, even those prepared by VPI. This higher activity would suggest that Tm may directly modify Pt or may even participate in accelerating the aromatization reaction.

However, the amount and method of incorporation of Tm is critical to the catalyst performance. While the sequential vapor-phase impregnation method with a small amount of Tm (0.15%) yielded a catalyst with improved catalytic properties, other methods such as coimpregnation of Pt and Tm hindered the dispersion of Pt, causing

blocking of the L-zeolite channels and a higher deactivation rate in the reaction

ACKNOWLEDGMENTS

This work was supported by the Oklahoma Center for the Advancement of Science and Technology (OCAST). We acknowledge the National Science Foundation for a GRT traineeship for G.J. and Phillips Petroleum for a scholarship. Support from NSF (Int. 9803052) is acknowledged. We also acknowledge the personnel at NSLS, Brookhaven National Laboratory, for the EXAFS experiments. A.B. is especially indebted to the Fundación Antorchas and the Fulbright Commission for financial support.

REFERENCES

1. Davis, R. J., "HCR Concise Review," p. 41, Wiley, New York, 1994.
2. Bernard, J. R., *in* "Proc. 5th Internat. Zeolite Confer." (L. V. C. Rees, Ed.), p. 686. Heyden, London, 1980.
3. Hughes, T. R., Buss, W. C., Tamm, P. W., and Jacobson, R. L., *in* "Proc. 7th Intern. Conf." (Murakami, *et al.* Eds.), p. 725. Kodansha, Tokyo, 1986.
4. McVicker, G. B., Kao, J. L., Ziemac, J. J., Gares, W. E., Robbins, J. L., Treacy, M. M. J., Rice, S. B., Vanderspurt, T. H., Cross, V. R., and Ghosh, A. K., *J. Catal.* **139**, 48 (1993).
5. Jacobs, G., Padro, C. L., and Resasco, D. E., *J. Catal.* **179**, 43 (1998).
6. Rotman, D., *Chem. Week* **8**, 150 (Feb. 26, 1992).
7. Vaarkamp, M., Miller, J. T., Modica, F. S., Lane, G. S., and Koningsberger, D. C., *J. Catal.* **138**, 675 (1992).
8. Fukunaga, T., and Ponec, V., *J. Catal.* **157**, 550 (1995).
9. Larsen, G., Haller, G. L., Resasco, D. E., and Durante, V. A., U.S. Patent 5,540,833 (1996).
10. Larsen, G., Resasco, D. E., Durante, V. A., Kim, J., and Haller, G. L., *Stud. Surf. Sci. Catal.* **83**, 321 (1994).
11. Landau, M. V., Kruglikov, V. Y., Goncharova, N. V., Konoval'chikov, O. D., Chukin, G. D., Smirnov, V. B., and Malevich, V. L., *Kinet. Catal.* **17**, 1104 (1976).
12. Frety, R., Da Silva, P. N., and Guenin, M., *Catal. Lett.* **3**, 9 (1989).
13. Miller, J. T., and Koningsberger, D. C., *J. Catal.* **162**, 209 (1996).
14. Li, F., Lu, W., Wu, G., and Li, J., *J. Alloys Compd.* **207/208**, 397 (1994).
15. Fang, X., Li, F., Zhou, Q., and Luo, L., *Appl. Catal. A* **161**, 227 (1997).
16. Grau, J. M., Daza, L., Seoane, X. L., and Arcoya, A., *Catal. Lett.* **53**, 161 (1998).
17. Fang, X., Li, F., and Luo, L., *Appl. Catal. A* **146**, 297 (1996).
18. Jacobs, G., Ghadiali, F., Pisanu, A., Borgna, A., Alvarez, W. E., and Resasco, D. E., *Appl. Catal. A: General* **188**, 79 (1999).
19. Ballatreccia, M., Zanoni, R., Dossi, C., Psaro, R., Recchia, S., and Vlaic, G., *J. Chem. Soc., Faraday Trans.* **91**, 2045 (1995).
20. Dossi, C., Psaro, R., and Zanoni, R., *J. Catal.* **159**, 435 (1996).
21. Mielczarski, E., Hong, S. B., and Davis, M. E., *J. Catal.* **134**, 349 and 359 (1992).
22. Alvarez, W. E., and Resasco, D. E., *Catal. Lett.* **8**, 53 (1991).
23. Treacy, M. M. J., *Microporous Mesoporous Mater.* **28**, 271 (1999).
24. Sayers, D. E., and Bunker, B. A., *in* "X-ray Absorption: Principles, Applications, Techniques of EXAFS, SEXAFS, and XANES" (D. Koningsberger and R. Prins, Eds.), p. 211. Wiley, New York, 1988.
25. Rehr, J. J., Zabinsky, S. I., and Albers, R. C., *Phys. Rev. Lett.* **69**, 3397 (1992).
26. Rehr, J. J., Mustre de Leon, J., Zabinsky, S. I., and Albers, R. C., *J. Am. Chem. Soc.* **113**, 5135 (1991).
27. Mustre de Leon, J., Rehr, J. J., Zabinsky, S. I., and Albers, R. C., *Phys. Rev. B* **44**, 4146 (1991).
28. Lane, G., Modica, F. S., and Miller, J. T., *J. Catal.* **129**, 145 (1991).
29. Brigham, E. O., "The Fast Fourier Transform," Prentice-Hall, Englewood Cliffs, NJ, 1974.
30. Stern, E. A., *Phys. Rev. B* **48**, 9825 (1993).
31. Newville, M., Ravel, B., Haskel, D., Stern, E. A., and Yacoby, Y., *Physica B* **208/209**, 154 (1995).
32. Koningsberger, D. C., and Gates, B. C., *Catal. Lett.* **14**, 271 (1992).
33. Vaarkamp, M., Modica, F. S., Miller, J. T., and Koningsberger, D. C., *J. Catal.* **144**, 611 (1993).
34. Jacobs, G., Alvarez, W. E., and Resasco, D. E., *Appl. Catal. A: General*, submitted.
35. Lane, G. S., Miller, J. T., Modica, F. S., and Barr, M. K., *J. Catal.* **141**, 465 (1993).
36. Stakheev, A. Y., Shpiro, E. S., Jaeger, N., I., and Schulz-Ekloff, G., *Catal. Lett.* **34**, 293 (1995).
37. Mojet, B. L., and Koningsberger, D. C., *Catal. Lett.* **39**, 191 (1996).
38. Iglesia, E., and Baumgartner, J. E., *in* "Proceedings, 10th International Congress on Catalysis, Budapest, 1992" (L. Guczi, F. Solymosi, and P. Tetenyi, Eds.), p. 993. Akad/miai Kiad[5], Budapest, 1993.
39. Iglesia, E., and Baumgartner, J. E., Proc. IX Internat. Zeolite Conf., Montreal, 1992.
40. Sharma, S. B., Ouraipryvan, P., Nair, H. A., Balaraman, P., Root, T. W., and Dumesic, J. A., *J. Catal.* **150**, 234 (1994).
41. Jentof, R. E., Tsapatsis, M., Davis, M. E., and Gates, B. C., *J. Catal.* **179**, 565 (1998).
42. Besoukhanova, C., Guidot, J., Barthomeuf, D., Breysse, M., and Bernard, J., *J. Chem. Soc., Faraday Trans. I* **77**, 1595 (1981).